

Atom–Molecule Coherence in a Bose-Einstein Condensate

Elizabeth A. Donley, Neil R. Claussen, Sarah T. Thompson, and Carl E. Wieman
JILA, University of Colorado and National Institute of Standards and Technology, Boulder, Colorado 80309-0440
(Dated: October 22, 2018)

Coherent coupling between atoms and molecules in a Bose-Einstein condensate (BEC) has been observed. Oscillations between atomic and molecular states were excited by sudden changes in the magnetic field near a Feshbach resonance and persisted for many periods of the oscillation. The oscillation frequency was measured over a large range of magnetic fields and is in excellent quantitative agreement with the energy difference between the colliding atom threshold energy and the energy of the bound molecular state. This agreement indicates that we have created a quantum superposition of atoms and diatomic molecules, which are chemically different species.

There is considerable interest in extending the applications of ultracold atoms to ultracold molecules. One route for producing a very cold and possibly Bose-condensed sample of molecules is to create the molecules from an atomic BEC. Wynar et al.¹ created cold $^{87}\text{Rb}_2$ molecules in a single ro-vibrational state of the ground-state potential from an ^{87}Rb BEC using a two-photon stimulated Raman transition. The authors could not probe the coherence properties of the molecules in that state, but the prospect of creating a superposition of atomic and molecular condensates initiated a flood of theoretical work on the subject^{2–6}. Ultracold molecules have also recently been formed through photoassociation of a sodium BEC⁷.

Utilizing the natural atom–molecule coupling that arises from a Feshbach resonance is an alternate route for producing ultracold molecules from an atomic BEC, and it is the route we have followed here. A Feshbach resonance is a scattering resonance for which the total energy of two colliding atoms is equal to the energy of a bound molecular state, and atom–molecule transitions can occur during a collision^{8–12}. A schematic representation of the potentials involved is shown in the inset of Fig. 1A. For our ^{85}Rb resonance, BEC atoms in the $F = 2$, $m_F = -2$ state collide on the open-channel threshold. F and m_F are the total spin and spin-projection quantum numbers. The bound state in the closed channel differs in energy by an amount ϵ from the open-channel threshold. The bound molecular wave function can be described as a sum of amplitudes of different hyperfine components (F , m_F) having $M_F = m_{F,1} + m_{F,2} = -4$ ¹³. Because of their different spin configurations, the atoms and molecules generally have different magnetic moments and the difference depends on magnetic field. Thus ϵ depends on magnetic field and the degree of atom–molecule coupling is magnetically tunable. The energy difference between the free atoms and the bound molecules is plotted in Fig. 1A. This behavior of the bound-state energy also causes a resonance in the scattering length, a , which is shown in Fig. 1B. The scattering length characterizes the mean-field interaction energy of a BEC.

When the magnetic field is tuned to values near the Feshbach resonance, theory predicts coherent oscillations

between the atomic and molecular states, but there is significant disagreement on the conversion fraction and the coherence properties^{16–21}.

In experiments with a sodium BEC, Stenger et al.²² observed that inelastic losses were dramatically enhanced when they ramped the magnetic field across the Feshbach resonance. We observed similar results for ^{85}Rb , but with lower rates^{23,24}. It is likely that the formation of molecules played a role in the loss, but there was no experimental evidence for the presence of molecules and the results followed a loss-rate dependence on time. More recently, we measured the time dependence of the loss in an ^{85}Rb BEC by applying controlled magnetic-field pulses toward but not across the Feshbach resonance²⁵. We observed the surprising result that under some conditions, shorter, more rapid pulses actually led to more loss than longer, slower pulses that spent more time near the resonance. The time dependence of the loss was suggestive of a nonadiabatic mixing of states, with the only states within a reasonable energy range being the normal atomic BEC state and the nearby bound molecular state.

In this work we show that much of the loss is likely due to the coherent mixing of atomic and molecular states. To create a superposition and probe its coherence, we applied two short magnetic-field pulses toward the Feshbach resonance, separated by a “free evolution” time during which the magnetic field was held at a constant value some distance from the resonance. We measured the number of atoms in the condensate as a function of time between the two pulses for various values of the steady-state magnetic field between the pulses. We observed dramatic oscillations in the number of atoms remaining in the atomic BEC at frequencies corresponding to the energy splitting between the molecular and the atomic states.

Experimental methods. The apparatus has been described in detail elsewhere^{23,25}. We first created ^{85}Rb condensates²³ typically containing 16,500 atoms, with fewer than 1,000 uncondensed thermal atoms. The initial number N_{init} fluctuated from shot to shot by ~ 500 atoms ($\sim 3\%$ number noise). After producing the condensate at a field of ~ 162 G, we ramped the magnetic field adiabatically to ~ 166 G, corresponding to an initial scattering

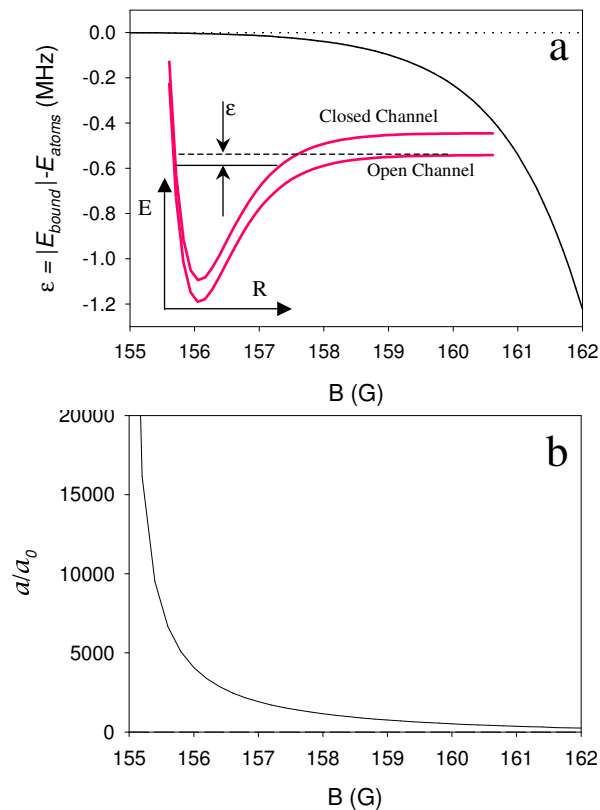


FIG. 1: Feshbach resonance bound-state energy and scattering length. (A) Energy splitting versus magnetic field. The resonance is centered at ~ 155 G. The solid curve is a theoretical estimate of the energy found with a coupled-channels calculation¹⁴, and the dotted line indicates $\epsilon = 0$. The inset schematically shows the collision channels involved in the resonance. ϵ depends on magnetic field because the atoms and molecules have different magnetic moments and thus the potentials have different Zeeman shifts. (B) Scattering length versus magnetic field for fields above the Feshbach resonance.

length $a_{init} \simeq 10 a_0$, where $a_0 = 0.053$ nm. The spatial distribution of the atoms was Gaussian with a peak atom density of $n_0 = 5.4 \times 10^{13} \text{ cm}^{-3}$, and the trap frequencies were $(17.4 \times 17.4 \times 6.8)$ Hz. After preparing the condensate we applied a selected fast magnetic-field pulse sequence by sending an appropriate time-dependent current through an auxiliary magnetic-field coil²⁵. A typical pulse sequence is shown in Fig. 2. It is composed of two nearly identical short trapezoidal pulses separated by a region of constant (but adjustable) magnetic field. Upon completion of the fast-pulse sequence in Fig. 2, we ramped the magnetic field from ~ 166 G to ~ 157 G in 5 ms and held at that field for an additional 7 ms to allow the repulsive mean-field energy to expand the condensate. Then we turned off the magnetic trap and used destructive absorption imaging 12.8 ms later to observe the atomic condensate and measure the number of remaining atoms²⁶. This detection scheme was nei-

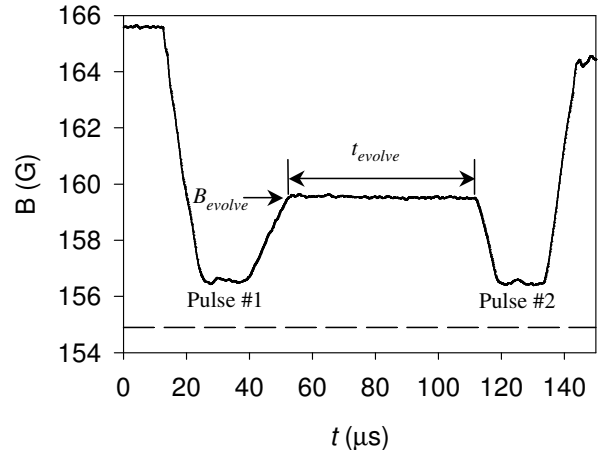


FIG. 2: Magnetic field pulse shape. Fields shown for pulses #1 and #2 correspond to scattering lengths of $\sim 2500 a_0$, and the free precession field B_{evolve} corresponds to a scattering length of $\sim 570 a_0$. The dashed line indicates the position of the Feshbach resonance. In the text, we refer to the free precession time as t_{evolve} . The rise/fall time for all of the pulses that we used was 14 μs .

ther sensitive to atoms with kinetic energies larger than $\sim 2 \mu\text{K}$ nor to atoms in off-resonant molecular states. We determined the value of the magnetic field between the pulses, B_{evolve} , by measuring the resonance frequency for transitions from the $F = 2, m_F = -2$ to the $F = 2, m_F = -1$ spin state by applying a 10 μs RF pulse to a trapped cloud of atoms²⁵.

Burst and remnant oscillations. As we observed for single pulses toward the Feshbach resonance²⁵, there were two distinct components of atoms observed in the absorption images and a third “missing” component that we could not detect. One of the observed components was a cold remnant BEC which was not noticeably heated or excited by the fast-pulse sequence, while the other component was a relatively hot (~ 150 nK) “burst” of atoms that remained magnetically trapped during the BEC expansion time. Using a variational approach²⁷ to model the mean-field expansion that we applied to the BEC remnant to measure its number, $N_{remnant}$, we found that we should impart ≤ 3 nK worth of energy to the remnant before imaging. This estimate agrees well with the expansion velocity that we observed after the trap turn-off. Thus the remnant BEC was nearly $50\times$ colder than the burst.

The missing component contained atoms that were in the initial sample but were not detected after the trap turn-off. To find the number of atoms in the remnant BEC and the number of burst atoms, we allowed the magnetic trap to “focus” the burst cloud before imaging²⁸. A typical image is shown in Fig. 3. We fit the focussed

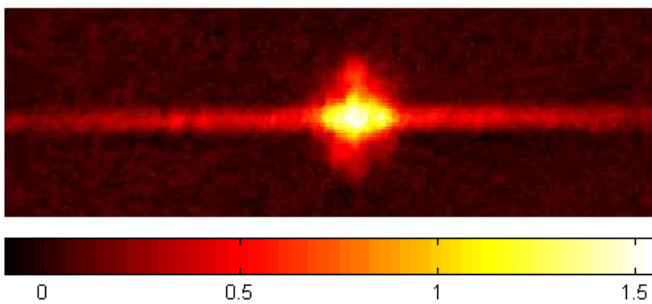


FIG. 3: An absorption image taken after the fast magnetic-field pulse sequence and the mean-field expansion. The color-bar indicates the optical density. The horizontal and vertical directions coincide with the axial and radial axes of the trap, respectively. The dimensions of the image are $366 \times 52 \mu\text{m}$. The BEC remnant is the roughly spherical cloud at the center, while the burst atoms are focussed into a thin line along the axial direction. Note the dramatic difference between the two spatial distributions, owing to the large difference in their mean energies ($\langle E_{burst} \rangle \simeq 50 \times \langle E_{remnant} \rangle$).

burst (which had a much larger spatial extent than the remnant) with a two-dimensional Gaussian surface, excluding the central region of the image that contained the remnant. This fit yielded the number of burst atoms, N_{burst} . Subtracting this fit from the image and performing a pixel-by-pixel sum of the central region of the image gave $N_{remnant}$.

$N_{remnant}$ versus t_{evolve} is plotted in Fig. 4 for two different values of B_{evolve} . The number clearly oscillates. Changing the value of B_{evolve} affected the oscillation frequency dramatically (note the change in scale from Fig. 4A to Fig. 4B). After only pulse #1 and the subsequent constant field but with no pulse #2, $N_{remnant}$ showed no variation except for a slow decay consistent with the loss rate expected for a single pulse to that field²⁵.

We have taken data similar to those in Fig. 4 for a variety of different B_{evolve} values. As in Fig. 4, we fit each curve to the function $y = y_0 + A \exp(-t/\tau) \sin(2\pi\nu t + \phi)$ to find the oscillation frequency ν and decay time constant τ . The measured frequencies are plotted versus B_{evolve} in Fig. 5 along with theoretical predictions for the bound-state energy relative to the atomic state.

In the regime where the scattering length is much larger than the radius of the interatomic potential well, the bound state energy for an arbitrary attractive potential can be approximated by $\epsilon = -\hbar^2/ma^2$ ²⁹. \hbar is Plank's constant divided by 2π , m is the atomic mass, and a is the scattering length. The same equation relates the bound state energy to the effective scattering length, which is calculated from the Feshbach resonance parameters through the relation $a = a_{bg} \times (1 - \frac{\Delta}{B-B_0})$, where a_{bg} is the background scattering length, Δ is the width of the Feshbach resonance, and B_0 is the resonant

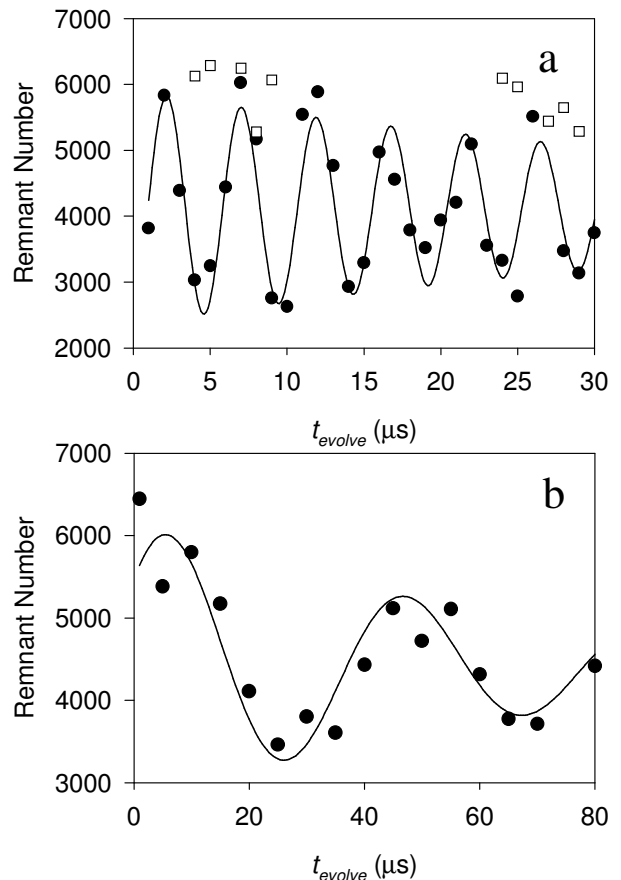


FIG. 4: $N_{remnant}$ versus t_{evolve} for $n_0 = 5.4 \times 10^{13} \text{ cm}^{-3}$. (A) $B_{evolve} = 159.69(4) \text{ G}$ ($a_{evolve} = 590 a_0$). The data fit to a damped sine wave with a frequency of $207(2) \text{ kHz}$ and a decay time of $46(21) \mu\text{s}$. The open squares near $N_{remnant} = 6000$ indicate the number remaining versus time after only pulse #1 and t_{evolve} at 159.69 G . (B) $B_{evolve} = 157.60(4) \text{ G}$ ($a_{evolve} = 1390 a_0$). Note the increase in time scale from (A). These data fit to an oscillation frequency of $23.9(12) \text{ kHz}$ and a decay time of $82(38) \mu\text{s}$.

magnetic field³⁰.

The quantity $|\epsilon|/\hbar$ is plotted with no adjustable parameters in Fig. 5. The measured oscillation frequencies are in excellent agreement with this simple model over the range of magnetic fields where the model is expected to be valid. The theoretical results found with a much more sophisticated coupled-channels scattering calculation¹⁴ in Fig. 5 are in excellent agreement with the data over the entire range.

The fact that the oscillations occurred at exactly the frequency corresponding to the bound-state energy clearly indicates that we are creating a coherent superposition of atoms and molecules with the sudden magnetic-field pulses^{11,12}. Although we do not have a detailed understanding of how the field pulses couple atoms and molecules, by choosing the shapes of the perturbing

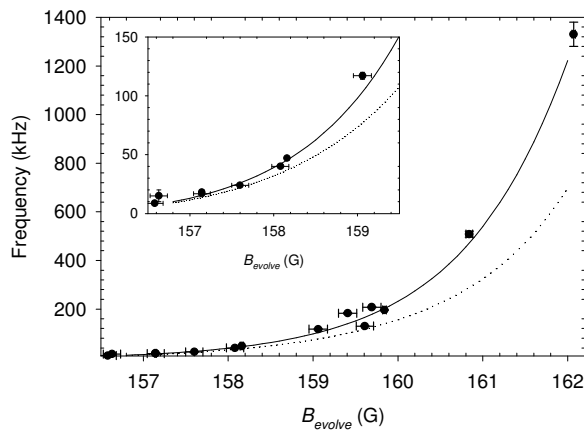


FIG. 5: Oscillation frequency versus magnetic field. The points are the measured frequencies. The solid line is the energy difference between the atom-atom threshold and the bound molecular state found by S. Kokkelmans with a coupled-channel scattering calculation. The dotted line is a plot of ϵ/h . The inset is an expanded view of the lower-frequency data. The maximum frequency that we could measure was limited only by timing jitter and finite resolution in the experiment. The magnetic-field measurements for the points with the smallest horizontal error bars were performed on the same days as the corresponding frequency measurements. The error bars for the points with larger field uncertainties were inflated by 100 mG to account for estimated day-to-day field drifts.

pulses such that a single pulse results in roughly 50% loss, we observe high-contrast oscillations in the number of atoms in the atomic BEC.

From the amplitude of the oscillations, one can put a lower bound on the number of molecules being created. Take, for example, the data in Fig. 4A. The amplitude of the atom oscillations was 1800(300) atoms. Assuming the fringes are coming from interference with molecules, there must be at least $1800/2 = 900(200)$ molecules on average. Assuming that the missing atoms are molecules that we fail to convert back into atoms gives an upper bound of 3200(100) molecules for the conditions of Fig. 4A.

The damping time for the oscillations, τ_{decay} , was more difficult to measure with high precision than the oscillation frequency. To within our measurement precision, τ_{decay} did not depend on B_{evolve} , but our uncertainties in τ_{decay} were as large as 100% for some fields. We had the highest precision measurements for frequencies around 200 kHz where the oscillation period was long compared to our experimental timing jitter but short compared to τ_{decay} . At frequencies near 200 kHz, we measured $\tau_{decay} = 38(8) \mu\text{s}$ for $n_0 = 1.3 \times 10^{14} \text{ cm}^{-3}$ and $\tau_{decay} = 91(33) \mu\text{s}$ when we decreased n_0 to $1.1 \times 10^{13} \text{ cm}^{-3}$.

N_{burst} also had interesting dependencies. For the conditions under which most of the data were collected,

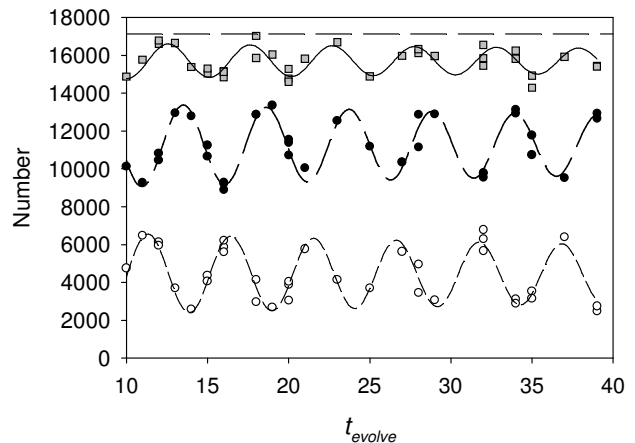


FIG. 6: Number versus t_{evolve} for $n_0 = 1.1 \times 10^{13} \text{ cm}^{-3}$. From bottom to top, the data are plots of N_{burst} (open circles), $N_{remnant}$ (filled circles), and the total number of observed atoms (gray squares). Each data set was fit to a damped sine wave resulting in the displayed fits. $N_{init} = 17,100$ is indicated by the flat dashed line. $B_{evolve} = 159.84(2) \text{ G}$ and the remnant data fit to an oscillation frequency of $196(1) \text{ kHz}$ and $\tau_{decay} = 91(33) \mu\text{s}$. To produce condensates with the lower density for these measurements, the fast-pulse sequence was applied from our evaporation field of 162.2 G and the amplitudes of pulses #1 and #2 were reduced to $\sim 7 \text{ G}$.

the burst contained ~ 5000 atoms on average, which is $\sim 30\%$ of N_{init} . N_{burst} depended on density and varied from one-half of the atoms lost from the condensate for our typical peak density of $n_0 = 5.4 \times 10^{13} \text{ cm}^{-3}$ to nearly all of the atoms lost from the condensate for $n_0 = 1.1 \times 10^{13} \text{ cm}^{-3}$. N_{burst} , $N_{remnant}$, and total number of atoms detected are plotted in Fig. 6 for $B_{evolve} = 159.84(2) \text{ G}$ and $n_0 = 1.1 \times 10^{13} \text{ cm}^{-3}$ ($5\times$ lower density than was used for the data shown in Fig. 4). All three components oscillated at the same frequency. The burst oscillation lagged behind the remnant oscillation by $155(4)^\circ$. Since the relative phase shift is nearly 180° , the oscillation amplitude for the total number was smaller than either the burst or the remnant amplitudes. The relative phase depended sensitively on the fall time of pulse #2. For example, when we increased the fall time from $11 \mu\text{s}$ to $159 \mu\text{s}$, the burst oscillation then lagged behind the remnant oscillation by $68(7)^\circ$ and the peak-to-peak amplitude of the total number oscillation was $5600(400)$.

For the conditions of Fig. 6, $N_{init} = 17,100$ exceeded the time-averaged total number of atoms counted after the pulse sequence by $8(3)\%$ on average. For the higher-density measurements in Fig. 4, $39(4)\%$ of the atoms were missing. Experiments with longer pulses #1 and #2 also had a higher fraction of missing atoms. For example, when we used $50 \mu\text{s}$ pulses with $n_0 = 5.4 \times 10^{13} \text{ cm}^{-3}$, $56(3)\%$ were missing.

We have carried out double-pulse measurements with a variety of widths and amplitudes for pulses #1 and #2 and a variety of different densities and initial magnetic fields. Although the oscillation frequency was unchanged, the phase, contrast, and damping of the oscillations did vary. The contrast was very sensitive to the pulse length, and was lower for longer pulses that created more missing atoms. Defining the contrast as the oscillation amplitude divided by the time averaged number of remnant atoms detected, we observed an optimum contrast of 0.42(7) for 15 μ s pulses to 156.6(1) G. A single such pulse removed about half of the atoms from the BEC. When the pulse length was comparable to τ_{decay} , the contrast was reduced by about a factor of two. Under those conditions, $\sim 3/4$ of the atoms were lost after pulse #1. The phase was shifted, but we did not observe a change in the contrast when we varied the amplitudes of pulses #1 and #2 from $B = 156.6(1)$ G ($2,400 a_0$) to $B = 155.1(1)$ G ($24,000 a_0$). The contrast did depend on the intermediate level, however, and was reduced for B_{evolve} values closest to the resonance, for which the magnetic-field jumps between B_{evolve} and pulses #1 and #2 were shortest.

We also looked for a temperature dependence of both the damping and the frequency at ~ 200 KHz and did not see any. The high-temperature data was much noisier than the data for pure condensates, due to unexplained enhanced noise in the number of thermal atoms after the magnetic-field pulse, but when the initial thermal fraction was increased from $<5\%$ to 30% , the data still fit to oscillations with frequency, amplitude, and damping consistent with what was observed with low temperature data.

Conclusions and Outlook. Our interpretation of our observations is that the first magnetic-field pulse provides a sufficiently rapid perturbation to result in nonadiabatic mixing between atomic and molecular states. The superposition then evolves according to the energy difference between the states, which is determined by the magnetic field during the free evolution stage, B_{evolve} . The second pulse mixes atom and molecule states again, such that the final state of the system depends on the relative phase of atomic and molecular fields at the time of the second pulse. This is somewhat analogous to Ramsey's method of separated oscillating fields³³. Under very limited conditions (a near $1700 a_0$), we could also observe Rabi-like oscillations with a single pulse towards the Feshbach resonance. This narrow window results from the conflicting needs for both strong coupling and condensate loss time²⁵ long compared to a Rabi oscillation period.

After pulse #2, a fraction of the coherent molecular component is converted into the energetic but still spin-polarized burst atoms through a yet to be determined process. Another mystery is the missing atoms. Are they molecules that are not converted back into atoms and are not detected in the burst or the remnant signals? If so, why do we not see them as atoms after the field is turned

off and the corresponding molecular state is no longer bound? Why are there fewer missing atoms for lower-density condensates and quicker pulses towards the Feshbach resonance? What is the actual conversion efficiency from atoms to molecules and how could we maximize it? Very near the Feshbach resonance, the molecular state has a magnetic moment nearly the same as that of the free atoms, and hence will remain magnetically trapped. A major remaining question concerns the nature of the molecules. Could they be considered a molecular BEC? Clearly there is much to be learned about this curious system.

1. Wynar, R. H., Freeland, R. S., Han, D. J., Ryu, C. & Heinzen, D. J. Molecules in a Bose-Einstein condensate. *Science* **287**, 1016-1019 (2000).
2. Heinzen, D. J., Wynar, R., Drummond, P. D. & Kheruntsyan, K. V. Superchemistry: dynamics of coupled atomic and molecular Bose-Einstein condensates. *Phys. Rev. Lett.* **84**, 5029-5033 (2000).
3. Anglin, J. R. & Vardi, A. Dynamics of a two-mode Bose-Einstein condensate beyond mean-field theory. *Phys. Rev. A* **64**, 013605/1-9 (2001).
4. Cusack, B. J., Alexander, T. J., Ostrovskaya, E. A. & Kivshar, Y. S. Existence and stability of coupled atomic-molecular Bose-Einstein condensates. *Phys. Rev. A* **65**, 013609/1-4 (2001).
5. Calsamiglia, J., Mackie, M. & Suominen, K. Superposition of macroscopic numbers of atoms and molecules. *Phys. Rev. Lett.* **87**, 160403-1 (2001).
6. Drummond, P. D., Kheruntsyan, K. V., Heinzen, D. J. & Wynar, R. H. Stimulated Raman adiabatic passage from an atomic to a molecular Bose-Einstein condensate. (available at <http://lanl.arxiv.org/abs/cond-mat/0110578>) 1-16 (2002).
7. McKenzie, C. *et al.* Photoassociation of Sodium in a Bose-Einstein Condensate. *Phys. Rev. Lett.* **88**, 120403/1-4 (2001).
8. Tiesinga, E., Moerdijk, A., Verhaar, B. J. & Stoof, H. T. C. Conditions for Bose-Einstein condensation in magnetically trapped atomic cesium. *Phys. Rev. A* **46**, R1167-R1170 (1992).
9. Tiesinga, E., Verhaar, B. J. & Stoof, H. T. C. Threshold and resonance phenomena in ultracold ground-state collisions. *Phys. Rev. A* **47**, 4114-4122 (1993).
10. Moerdijk, A. J., Verhaar, B. J. & Axelson, A. Resonances in ultracold collisions of ^6Li , ^7Li , and ^{23}Na . *Phys. Rev. A* **51**, 4852-4861 (1995).

11. van Abeelen, F. A. & Verhaar, B. J. Time-dependent Feshbach resonance scattering and anomalous decay of a Na Bose-Einstein condensate. *Phys. Rev. Lett.* **83**, 1550-1553 (1999).
12. Mies, F. H., Tiesinga, E. & Julienne, P. S. Manipulation of Feshbach resonances in ultracold atomic collisions using time-dependent magnetic fields. *Phys. Rev. A* **61**, 022721/1-17 (2000).
13. van Abeelen, F. A., Heinzen, D. J. & Verhaar, B. J. Photoassociation as a probe of Feshbach resonances in cold-atom scattering. *Phys. Rev. A* **57**, R4102-R4105 (1998).
14. The coupled-channels calculations were kindly provided by Servaas Kokkelmans and Chris Greene. The calculations used the best estimates of the Feshbach resonance parameters found by combining the results of three high-precision experiments. The determination of the parameters and the construction of the potentials is described in detail by van Kempen et al.¹⁵
15. van Kempen, E. G. M., Kokkelmans, S. J. J. M. F., Heinzen, D. J. & Verhaar, B. J. Interisotope determination of ultracold rubidium interactions from three high-precision experiments. *Phys. Rev. Lett.* **88**, 093201/1-4 (2002).
16. Timmermans, E., Tommasini, P., Hussein, M. & Kerman, A. Feshbach resonances in atomic Bose-Einstein condensates. *Phys. Rep.* **315**, 199-230 (1999).
17. Timmermans, E., Tommasini, P., Côté, R., Hussein, M. & Kerman, A. Rarified liquid properties of hybrid atomic-molecular Bose-Einstein condensates. *Phys. Rev. Lett.* **83**, 2691-2691 (1999).
18. Drummond, P. D., Kheruntsyan, K. V. & He, H. Coherent molecular solitons in Bose-Einstein condensates. *Phys. Rev. Lett.* **81**, 3055-3058 (1998).
19. Holland, M., Park, J. & Walser, R. Formation of pairing fields in resonantly coupled atomic and molecular Bose-Einstein condensates. *Phys. Rev. Lett.* **86**, 1915-1918 (2001).
20. Góral, K., Gajda, M. & Rzążewski, K. Multimode dynamics of a coupled ultracold atomic-molecular system. *Phys. Rev. Lett.* **86**, 1397-1401 (2001).
21. Vardi, A., Yurovsky, V. A. & Anglin, J. R. Quantum effects on the dynamics of a two-mode atom-molecule Bose-Einstein condensate. *Phys. Rev. A* **64**, 063611/1-5 (2001).
22. Stenger, J. *et al.* Strongly enhanced inelastic collisions in a Bose-Einstein condensate near Feshbach resonances. *Phys. Rev. Lett.* **82**, 2422-2425 (1999).
23. Cornish, S. L., Claussen, N. R., Roberts, J. L., Cornell, E. A. & Wieman, C. E. Stable ⁸⁵Rb Bose-Einstein condensates with widely tunable interactions. *Phys. Rev. Lett.* **85**, 1795-1798 (2000).
24. Claussen, N. R., Cornish, S. L., Roberts, J. L., Cornell, E. A. & Wieman, C. E. in *Atomic Physics 17*, (ed. Arimondo, E., DeNatale, P., & Inguscio, M.) 325-336 (American Institute of Physics, New York, 2001).
25. Claussen, N. R., Donley, E. A., Thompson, S. T. & Wieman, C. E. Microscopic Dynamics in a Strongly Interacting Bose-Einstein Condensate. in press (available at <http://lanl.arxiv.org/abs/cond-mat/0201400>) 1-4 (2002).
26. Roberts, J. L. *et al.* Controlled collapse of a Bose-Einstein condensate. *Phys. Rev. Lett.* **86**, 4211-4214 (2001).
27. Pérez-García, V. M., Michinel, H., Cirac, J. I., Lewenstein, M. & Zoller, P. Dynamics of Bose-Einstein condensates: variational solutions of the Gross-Pitaevskii equations. *Phys. Rev. A* **56**, 1424-1432 (1997).
28. Donley, E. A. *et al.* Dynamics of collapsing and exploding Bose-Einstein condensates. *Nature* **412**, 295-299 (2001).
29. Sakurai, J. J. *Modern Quantum Mechanics* (Addison-Wesley, Reading, Massachusetts, 1994).
30. Rethermalization measurements in ⁸⁵Rb thermal clouds yield values of $B_0 = 154.9(4)$ G and $\Delta = 11.0(4)$ G (31). The best estimate of a_{bg} is an estimate found by mass scaling spectroscopic measurements of the four highest-lying bound states of ⁸⁷Rb¹⁵, which gives $a_{bg} = -450(3) a_0^{32}$.
31. Roberts, J. L. *et al.* Improved characterization of elastic scattering near a Feshbach resonance in ⁸⁵Rb. *Phys. Rev. A* **64**, 024702/1-3 (2001).
32. Kokkelmans, S. J. J. M. F. Private Communication.
33. Ramsey, N. F. A molecular beam resonance method with separated oscillating fields. *Phys. Rev.* **78**, 695-699 (1950).

Acknowledgements

We would like to acknowledge contributions from E. A. Cornell and the JILA quantum gas collaboration. We are particularly grateful to C. H. Greene and S. J. J. M. F.

Kokkelmans for providing us with the coupled-channel scattering calculations presented in Fig. 4 and to L. Pitaevskii for numerous fruitful discussions. S. T. T. acknowledges the support of an ARO-MURI Fellowship. This work was also supported by ONR and NSF.

Correspondence and requests for materials should be addressed to N.R.C.

(e-mail:nclausse@jilau1.colorado.edu.)